X-ray spectroscopy of interstellar dust: from the laboratory to the Galaxy

Zeegers, S.T.

4 X-ray extinction from interstellar dust

Abstract

Aims We present a study on the prospects of observing carbon, sulfur, and other lower abundance elements (namely Al, Ca, Ti and Ni) present in the interstellar medium using future X-ray instruments. We focus in particular on the detection and characterization of interstellar dust along the lines of sight.

Methods We compare the simulated data with different sets of dust aggregates, either obtained from past literature or measured by us using the SOLEIL-LUCIA synchrotron beamline. Extinction by interstellar grains induces modulations of a given photoelectric edge, which can be in principle traced back to the chemistry of the absorbing grains. We simulated data of instruments with characteristics of resolution and sensitivity of the current *Athena*, XARM and Arcus concepts.

Results In the relatively near future, the depletion and abundances of the elements under study will be determined with confidence. In the case of carbon and sulfur, the characterization of the chemistry of the absorbing dust will be also determined. For aluminum and calcium, despite the large depletion in the interstellar medium and the prominent dust absorption, in many cases the edge feature may not be changing significantly with the change of chemistry in the Al- or Ca- bearing compounds. The extinction signature of large grains may be detected and modeled, allowing a test on different grain size distributions for these elements. The low cosmic abundance of Ti and Ni will not allow us a detailed study of the edge features.

E. Costantini, S.T. Zeegers, D. Rogantini, C.P. de Vries, A.G.G.M. Tielens, L.B.F.M. Waters

Submitted to A&A

4.1 Introduction

Absorption and scattering in the X-ray band has proved a useful diagnostic of the interstellar dust (ID) properties. By virtue of the broad band coverage, the X-ray band displays many photoelectric absorption edges, caused by the mixture of gas and dust intervening along the line of sight towards bright background sources (Draine, 2003; Hoffman and Draine, 2016). Absorption by interstellar grains is detected as a result of the interaction between the incoming X-ray photon and the electrons inside the grain's atoms. The multiple-generated photoelectron-waves interfere with each other both constructively and destructively. This interference pattern depends on the complexity of the chemical compound and the distance of the electrons from the nucleus. Each pattern is a fingerprint of a given material (Rehr and Albers, 2000). The extinction cross section, the sum of the absorption and scattering cross section (e.g., Draine, 2003; Corrales et al., 2016) in the X-ray band, provides, in principle, not only direct estimate on the chemistry of the interstellar medium (ISM), but also information on the size distribution, crystallinity and porosity of the intervening grains (Hoffman and Draine, 2016; Zeegers et al., 2017; Rogantini et al., 2018). In recent years, the deep features of the Fe L and O K and Si K-edges have been studied using the grating spectrometers on board the X-ray Observatories *Chandra* and XMM-*Newton*. These studies made use of absorption profiles either taken from the literature (Costantini et al., 2012; Pinto et al., 2010, 2013; Valencic and Smith, 2013) or obtained with dedicated synchrotron measurements (Lee et al., 2009; Zeegers et al., 2017).

Outside the energy band where the sensitivity and resolution of the current instruments is maximized, it is at this moment challenging to study interstellar dust. An example is given by the tentative study of the C K-edge (Schneider and Schmitt, 2010), which was severely hampered by various instrumental effects, although the carbon edge would formally be included in the energy range of *Chandra*-LETGS.

In this chapter, we investigate the prospective of observing and modeling the elements of the ID which have not been yet studied, which happen to fall in the 1.5–8.3 keV band (Al, S, Ca, Ti, Ni) and at E<0.5 keV (carbon).

In Fig. 4.1 we show the abundance pattern of the photoelectric absorption edges of the elements (with atomic number A=6-30) as a function of the X-ray energy. The empty diamonds mark the edges that have been already studied by current instruments unveiling the dust features: the O K and Fe L-edges at 0.534 and 0.7 keV respectively (Lee et al., 2009; Costantini et al., 2012; Pinto et al., 2010, 2013; Valencic and Smith, 2013); the Mg and Si K-edges at 1.3 and 1.84 keV respectively (Zeegers et al., 2017, Rogantini et al. in prep.). The black triangles mark the edges presented in this work. We present the Fe K-edge, marked with a light gray triangle in the figure, in a separate paper (Rogantini et al., 2018), but see also (Lee and Ravel, 2005). The middle panel shows the range of depletion, defined as the amount of dust over the total amount of matter in the ISM (dust and gas) that is expected for a given element. The wide range of depletions for some elements is due to the different density environments where those are observed (e.g., Jenkins, 2009).

In the lower panel of Fig. 4.1 we show the energy range of present and future missions. The solid line highlights the region where the instrument capabilities (resolution and effective

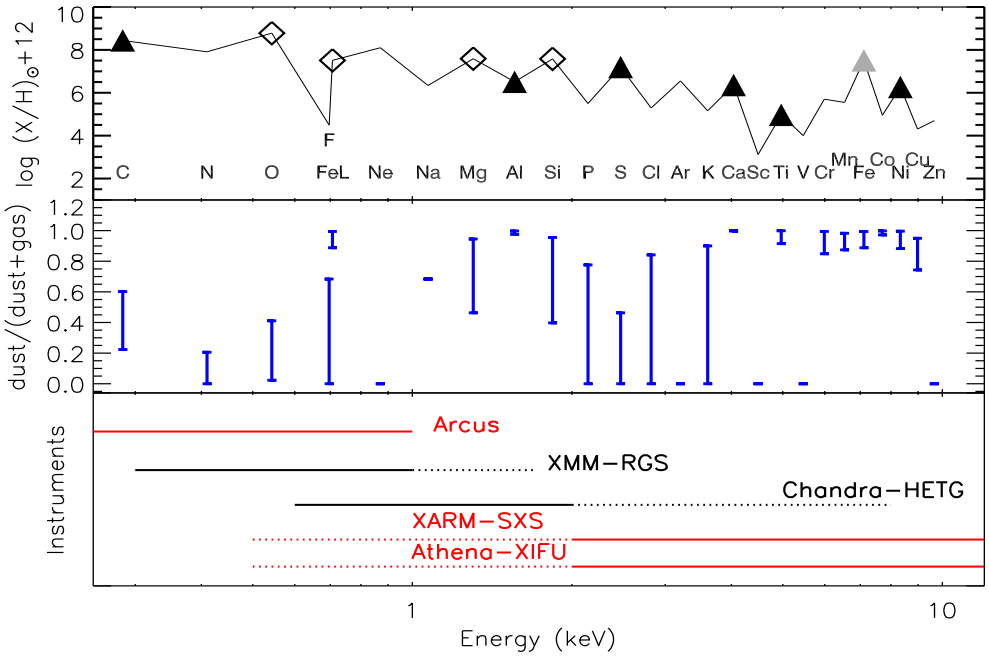

Figure 4.1: Upper panel: abundance pattern as a function of energy for the absorbing elements in the X-ray band. The K-edge energy is indicated, except from Fe, for which both the K- and the L-edges, at 7.1 and ~0.7 keV, respectively, can be studied. Abundances follow Lodders (2010) and they are expressed in terms of log (X/H)+12. In this frame, the abundance of hydrogen is 12. The open diamond mark the elements that are accessible by current instruments. The triangles are the relevant elements that will be accessible by future instruments to study dust. The black triangles are the subject of this work. Middle panel: range of depletions as reported by Jenkins (2009) for all elements, except: C (Jenkins, 2009; Whittet, 2003), F (Snow et al., 2007), Na (Turner, 1991), S (Gry and Jenkins, 2017), K (Snow, 1975), Ca (Crinklaw et al., 1994), Co (Federman et al., 1993), Al (Jenkins and Wallerstein, 1996), Ar (Sofia and Jenkins, 1998). Lower panel: energy range covered by present and future (red) missions. The solid line highlights the energy range where the capabilities of the instruments are optimal for observing absorption by dust.

area) are optimal to observe the dust absorption features. The *Chandra* and XMM-*Newton* observatory (both launched in 1999, Weisskopf, 1999; Jansen et al., 2001) are still in operation. The grating spectrometer Arcus will cover the soft X-ray range (Table 4.2). It is a NASA mission currently in the study phase, with a possible launch date of 2023 (Smith et al., 2016). The calorimeter on board of the X-ray Astronomy Recovery Mission (XARM, to be launched around 2020)[1] is planned to have the same characteristics of the one on board of the lost *Hitomi* satellite (Mitsuda et al., 2014). Finally, we display the energy coverage of the *Athena* calorimeter XIFU (Barret et al., 2016), to be launched in 2030. Both XARM and *Athena*'s calorimeter will be optimal to observe the higher energy dust features (Table 4.2).

4.1.1 The elements in this study

One of the major players in the ID, carbon, constitutes around 20% of the total depleted mass in the Galaxy (Whittet, 2003). Its depletion covers a relatively narrow range of values, (Figure 4.1) showing that it is not a strong function of environmental density. It has been hypothesized that the majority of carbon should be locked in graphite grains, as a likely explanation for the 2175 Å emission feature (Draine, 1989, 2003, and references therein). Graphite has been commonly adopted in ID models (e.g., Mathis et al., 1977). However, observational evidences pointed out that graphite could not explain the variability of the 2175 Å feature (Fitzpatrick and Massa, 2007). Furthermore, in analogy with the silicates, which are found to be amorphous, also graphite was deemed unlikely to survive in large quantities in the harsh environment of the ISM. Graphite should therefore face a natural process of amorphisation (Compiègne et al., 2011).

The idea of carbon as a single and separate phase from the silicate population does not agree with a scenario of a constantly evolving and mixing medium (Jones et al., 2017). Hydrogenated Amorphous Carbon (HAC) may indeed coat the silicate grains, forming a single population (e.g., Duley et al., 1989), with different characteristics with respect to the environment where they reside and depending on the particle size (e.g., Jones et al., 2017, and references therein). However, this scenario has so far not been confirmed by polarization studies. The carbon feature at 3.4 μm shows a negligible degree of polarization with respect to the silicate feature at 9.7 μm, pointing to two distinct grain populations (Whittet, 2011).

Finally, under special condition of high pressure, for instance in a shocked environment, graphite and amorphous carbon can turn into nano-diamonds, which can constitute as much as 5% of the amount of C in the ISM (Tielens et al., 1987), possibly with H and N inclusion (Van Kerckhoven et al., 2002; Bilalbegović et al., 2018). Diamonds of possible ISM origin have been found in meteorites (Lewis et al., 1987). An important carbon carrier are Polycyclic Aromatic Hydrocarbons (PAH), large (Å-sized) molecules formed by carbon and hydrogen in a honeycomb structure. They constitute up to about 10% of the carbon abundance (e.g., Tielens, 2013). PAHs are quite sensitive to ionizing radiation from far-ultraviolet to X-rays and they are easily destroyed near star formation sites at AU distance scale (e.g., Siebenmorgen and Krügel, 2010), up to kpc scale, for active galaxies (Voit, 1992).

A part from C, other constituents can be studied in detail by future generation telescopes.

Sulfur in dust phase seems to be absent from the diffuse ISM (Sembach and Savage, 1996). However, a relative fast transition to a depletion approaching -1 dex is reported in

[1] the XARM mission has been recently renamed XRISM (X-Ray Imaging Spectroscopy Mission)

dense media, such as molecular clouds (Joseph et al., 1986). In molecular clouds, sulfur can be included in aggregates such as H_2S, SO_2, OCS, SO, H_2CS, NS SiS, CS, HNCS, CH_3SH (Duley et al., 1980, and references therein) as well as other carbon-hydrogen bearing sulfates (e.g., Bilalbegović and Baranović, 2015). Molecular reactions may also lead to sulfur aggregation into polymeric forms, like S_8 (e.g., Jiménez-Escobar and Muñoz Caro, 2011). However, even integrating the contribution of all S-bearing molecules, the absolute abundance of sulfur in molecular clouds compared to the diffuse ISM one, with a ratio of $\sim 10^{-8}/10^{-5}$ is inexplicably low (Wakelam and Herbst, 2008). Inclusion into simple atomic sulfur or sulfur ices have been proposed to solve the missing-sulfur problem in molecular clouds (e.g., Vidal et al., 2017).
Sulfur in dust has been also detected near C-rich AGB stars, planetary nebulae (Hony et al., 2002) and protoplanetary disks (Keller et al., 2002), predominantly in form of troilite (FeS). Finally, sulfur is abundant in solid form in planetary systems bodies, such as interplanetary dust particles, meteorites and comets (e.g., Wooden, 2008, and references therein).
The presence of sulfur in dust form in the ISM has been suggested in association with GEMS (Glasses with Embedded Metal and Sulfides, Bradley, 1994), where the FeS particles would be more concentrated on the surface of the glassy silicate. However, the majority of GEMS may well be of nebular origin, rather than the ISM (Keller and Messenger, 2008). Sulfur in FeS, consistent to be of ISM origin, has been recorded in the data from the Stardust mission (Westphal et al., 2014). This evidence revitalizes the idea of the presence of sulfur in dust-form also in less dense environments of the ISM. The presence of strong UV radiation and cosmic rays has been thought to be the cause for the extreme sputtering of the highly volatile S, for example from GEMS surfaces. Recent experiments however put to the test this hypothesis (Keller et al., 2010), showing that UV bombardment has in fact little influence on sulfur stuck on a grain surface.

Aluminum, calcium and titanium are extremely depleted in the ISM (Fig. 4.1). Ca and Ti show also a very similar depletion pattern as a function of gas density (Crinklaw et al., 1994). These two elements are found in gas only in tenuous environments, associated with warm inter cloud media in both the halo (Edgar and Savage, 1989) and the disk of the Galaxy (Crinklaw et al., 1994). The depletion of Ti is severe, regardless of the environment, ranging between -1 dex and -3.1 dex (Welty and Crowther, 2010). The ratio of column density between Ti II and Ca II, representative of the element neutral gas phase, is in general constant in the Galaxy (~0.4, Hunter et al., 2006). Al, Ca and Ti have a similar condensation temperature (1400–1600 K, Field, 1974) and it has been hypothesized that, being the first to form in e.g., a stellar envelope or a supernova environment, they would form the core of complex dust grains with silicate and possibly ice mantles (e.g., Clayton, 1978). This would provide a natural shield for these Al, Ca, Ti-bearing compounds, preventing their destruction and ensuring a high depletion in the vast majority of the environments. Under the condition of thermodynamic equilibrium, aluminum first condenses in Al_2O_3. From there it may evolve into spinel ($MgAl_2O_4$) and eventually into a Ca and Al-bearing silicate. The latter are stable compounds, thanks to very high binding energies (Trivedi and Larimer, 1981). Calcium is mostly locked in dust in silicates (e.g., $CaMgSi_2O_6$, Field, 1974; Trivedi and Larimer, 1981). Calcium carbonates, possibly formed in AGB stars envelopes (e.g., Kemper et al., 2002), are believed to be unstable and therefore Ca inclusion in silicates, which form already at high temperatures, are favored (Ferrarotti and Gail, 2005). Titanium is produced by AGB stars mostly

Table 4.1: Samples of interstellar dust analogues used in this work

Specie	Name	atom	Ref	E_{SPEX} (eV)	E_{Henke} (eV)
C	graphite	C	Albella and Banks (1998)	2880	2842
AC	amorphous carbon	C	Albella and Banks (1998)		
HAC	hydrogenated amorphous carbon	C	Buijnsters et al. (2009)		
C	diamond	C	Albella and Banks (1998)		
$MgAl_2O_4$	spinel	Al	this work	1564	1559
Al_2O_3	aluminum oxide	Al	this work		
FeS_2	pyrite	S	Bonnin-Mosbah et al. (2002)		
FeS	troilite	S	[1]		
$Fe_{0.875}S$	pyrrhotite	S	[1]		
$CaMgSi_2O_6$	diopside crystal	Ca	Neuville et al. (2007)	4041	4038
$CaMgSi_2O_6$	diopside glass	Ca	Neuville et al. (2007)		
$Ca_3Al_2O_6$	tricalcium aluminate	Ca	Neuville et al. (2007)		
$CaAl_2O_4$	calcium aluminate	Ca	Neuville et al. (2007)		
TiO_2	titanium dioxide	Ti	Shin et al. (2013)	[2]	4966
Ni	metallic nickel	Ni	Van Loon et al. (2015)	8338	8331

[1] http://www.esrf.eu/home/UsersAndScience/Experiments/XNP/ID21/php/DatabaseSCompounds.html

[2] the Ti edge is not by default implemented in the SPEX model.

in the form of TiO_2, which constitute a seed nucleus later included in the larger/coated grains (e.g., Ferrarotti and Gail, 2006).

Nickel depletion is found to correlate with the one of Fe for a variety of environments, from planetary nebulae (Delgado-Inglada et al., 2016) to diffuse interstellar clouds (Jenkins, 2009). These two elements display a similar condensation temperature (1336 and 1354 K for Fe and Ni, respectively Wasson, 1985), which already point to a simultaneous inclusion into dust grains. However, it has been observed that in dense environments Ni is more depleted than Fe (e.g., Sembach and Savage, 1996; Delgado-Inglada et al., 2016).

4.2 Extinction profiles

In this chapter, we make use of literature values to infer the absorption absolute cross sections for all elements, except for Al (Sect. 4.2.1). Measurements of X-ray edges profiles are mostly carried out for industry and are rarely of interest for astronomical applications. For this reason, the sample selection is bound to be incomplete. The compounds used are listed in Table 4.1. We follow closely the method presented in Chapter 2 and Rogantini et al. (2018) to obtain the extinction profiles to be confronted to the astronomical data. The laboratory data are transformed to transmission spectra and matched (via χ^2 fitting) to tabulated transmission data of the same compound, where we assume an optically thin sample, as to mimic the conditions in the ISM. The transmission tables are provided by the Center for X-ray Optics at Lawrence Berkeley National laboratory based on tabulated data by Henke et al. (1993). From the trans-

mission spectra, the attenuation coefficient can be obtained and consequently we can obtain the imaginary part of the refractive index from this coefficient. The real part of the refractive index m, is calculated via the Kramers-Kronig relations (Bohren, 2010). The knowledge of m is needed in order to calculate the extinction cross section to involve both the effect of absorption and scattering. The extinction cross sections are calculated using Mie theory (Mie, 1908; Wiscombe, 1980) for C, Al and S. We used instead the anomalous diffraction theory (ADT, Van der Hulst 1957) for Ca, Ti and Ni. The ADT theory can be used when the ratio $x = 2\pi a/\lambda \gg 1$ where a is the grain size and λ is the wavelength of the incident radiation. In order to obtain the extinction cross section for a range of dust grain radii, we assume the MRN size distribution (Mathis et al. 1977). The grain size is weighted by a power law of slope -3.5 within a grain size range 0.025-0.25 μm. Once the absolute cross section as a function of energy has been obtained, we implemented the extinction profiles in the already existing AMOL model in the fitting code SPEX (ver. 3.03, Kaastra et al., 1996). We note however that the edge energy as tabulated by Henke et al. (1993), may differ from the Verner cross sections implemented in SPEX (Verner et al., 1996). In this chapter, we apply a shift to the laboratory data in order to consistently compare them with the edge features as seen by SPEX. Those shifts are sometimes noticeable (Table 4.1).

4.2.1 Laboratory data for aluminum

For Al, we made use of the laboratory data that we collected at the LUCIA beamline at the Soleil synchrotron facility. Both the samples, Al_2O_3 and $MgAl_2O_4$, were commercially available from the Alfa-Aesar and Aldrich company, respectively. The samples, in powder form, were pressed on thin indium foil, placed on a copper support which was placed in a vacuum environment. The sample was then irradiated by an X-ray beam of which the energy is tuneable. The X-ray fine structures were measured through fluorescence. At these soft X-ray energies, this method is more practical than the more intuitive method of measuring the transmission through the sample, because for transmission measurements the samples have to be too thin to be easily handled. The fluorescent method to obtain the XAFS does require a correction for possible saturation. This correction was performed with the program FLUO, which is part of the UWXAFS software (Stern et al., 1995). A full description of the procedure for the analysis of the data can be found in Chapter 2.

4.3 Simulations

We present the prospects of detecting absorption K-edges relevant for dust studies using future missions (Fig. 4.1). The only instrument proposed for studying the soft X-ray energy band is, at this moment, the Arcus grating spectrometer[2] (Smith et al., 2016). For the energy above ~2 keV, two microcalorimeters will provide an unprecedented resolution: *Resolve* and XIFU, on board of XARM[3] and *Athena*[4] (Nandra et al., 2013), respectively. The effective area and the resolving power of these three instruments at the energy of the features studied here are

[2] http://www.arcusxray.org/

[3] https://heasarc.gsfc.nasa.gov/docs/xarm/

[4] http://www.the-athena-x-ray-observatory.eu/

reported in Table 4.2. With the chosen exposure time, we would obtain an associated error on the dust or gas column density of around 1% for C (Arcus) Al, S and Ca (XIFU).

The simulations were carried out having in mind realistic scenarios in our Galaxy, in order to prove the effective prospect of future instruments to measure physical parameters. We first simulated the data, considering the different instruments responses and including noise, assuming first that the photoelectric edge is only due to gas absorption. These simulations are confronted with models, folded with the appropriate response, which include an amount of gas set by the typical depletion found in the literature for a given element plus the contribution of a dust compound. We adopted the MRN dust size distribution in all cases (Mathis et al., 1977). However, the exceptional depletion of Al and Ca, joint to favorable observing conditions allowed us to test also the detectability of a distribution where the mass distribution is skewed towards larger grains (Draine and Fraisse, 2009). This distribution has a size range of $a = 0.02 - 1\,\mu$m, with an average grain size of $0.6\,\mu$m. The observing conditions are favorable for these two elements first because the brightness of the sources with a favorable $N_{\rm H}$ is often high (e.g., low mass X-ray binaries, LMXB, near the galactic center) and, second, the edges fall in a large effective-area region of the instrument.

The depletion of carbon has been optimistically assumed to be 0.6, but still implies a substantial role in gas absorption in the carbon edge. For this reason, although the edge feature itself can also be detected at relatively small column density (e.g., $N_{\rm H} \sim 10^{20}\,{\rm cm}^{-2}$), a much larger amount of matter is necessary to make the dust features evident. Here we simulated a column density of $N_{\rm H} = 1.6 \times 10^{21}\,{\rm cm}^{-2}$ for a flux in the soft energy band of $\sim 3 \times 10^{-9}\,{\rm erg\,cm}^{-2}\,{\rm s}^{-1}$ (Fig. 4.2). Note that for this column density, the C I absorption lines from gas are already saturated (Fig. 4.2), therefore they cannot be used straightforwardly to measure depletion. Although this value for a column density is not uncommon for LMXB, the source needs to be in an hypothetical high state to be well detected by an Arcus-like instrument as the effective area of such an instrument would fall rapidly at the carbon edge.

The cosmic abundance of Al is significantly less than the main ID components (Fig. 4.1). However, Al in the ISM is almost completely depleted into dust. We simulate here the contribution of Al_2O_3 and $MgAl_2O_4$ and compare them with a theoretical pure gas absorption (Fig. 4.3). At ISM temperature, Al, if it was totally in gas form, would be distributed between Al I and Al II. For this simulation, we selected the bright LMXB ($F_{2-10\,{\rm keV}} \sim 3 \times 10^{-9}\,{\rm erg\,cm}^{-2}\,{\rm s}^{-1}$) GX 3+1 whose spectral parameters where obtained from *Chandra*-HETGS data (obsid 16492).

For the sulfur simulation (see Figure 4.4), we selected GX 5-1, which is among the brightest LMXB in the Galaxy, with a $F_{2-10\,{\rm keV}} \sim 2.5 \times 10^{-8}\,{\rm erg\,cm}^{-2}\,{\rm s}^{-1}$. The hydrogen column density is about $3.4 \times 10^{22}\,{\rm cm}^{-2}$ (Zeegers et al., 2017). The depletion of sulfur is unknown in the diffuse ISM, but it has been estimated that could be up to ~46% (Fig. 4.1 and Gry and Jenkins, 2017). Here we simulate a more conservative 30% depletion. Given the relatively low depletion of S, the XAFS features (Fig. 4.8) would be less evident in the data.

The X-ray spectrum will be sensitive to calcium extinction only if the intervening column density is sufficiently high. This is due to the relatively high energy position of the photoelectric edge. Here we simulated GX 340+00 ($F_{2-10\,{\rm keV}} \sim 2.5 \times 10^{-8}\,{\rm erg\,cm}^{-2}\,{\rm s}^{-1}$), with a column density of about $N_{\rm H} \sim 6.9 \times 10^{22}\,{\rm cm}^{-2}$, obtained from HETG-*Chandra* data fitting (obsid 6632).

For both titanium and nickel, we simulated a hypothetical source, for example near the

Table 4.2: Parameters of the instruments used in the simulations at the energy of the elements studied here.

Element	R E/ΔE	A_E^{Eff} cm^2	Inst.
C	2540	390	Arcus
Al	596	13898	XIFU
S	911(455)	7335(209)	XIFU(Resolve)
Ca	1545(772)	5471(271)	XIFU(Resolve)
Ti	1940	4211	XIFU
Ni	3290	1100	XIFU

GC, where also the occurrence of high column density molecular clouds is more frequent, that in outburst reaches a flux as high as GX 340+00. The column density must be sufficient to produce an edge-like modulation in the spectrum ($N_{\rm H} \sim 1.3 \times 10^{23}$ cm^{-2}).

4.4 Discussion

4.4.1 Carbon

In the simulation (see Figure 4.2), we included gas and the carbon forms that are believed to be most abundant (namely graphite, amorphous carbon and HAC). While the difference between graphite and amorphous carbon is subtle, HAC does have more distinctive features that may be more easily detected. The hydrogenation of carbon may point to either an environment protected from strong radiation or the presence of large grains, which are more resilient to radiation (Sect. 4.1.1).

For illustrative purposes, we also include diamonds (orange dashed line) in order to show the departure of this form of carbon from the shape of e.g., graphite. However, in practice, diamonds are believed to constitute no more than 5% of the carbon (Tielens, 2001). Its realistic inclusion would be non-detectable (dashed-dotted blue line in Figure 4.2). The same negligible effect may be produced by PAH, which we did not include in our simulation. The total amount along a line of sight is relatively low (Sect. 4.1.1) and the spectral features of PAH would be mixed with a more dominant amorphous carbon (or graphite) contribution. The sparse historical studies of PAH absorption profiles for the X-ray region have been recently revived (Reitsma et al., 2014, 2015). This will help in defining a shape for the summed contribution of the numerous different PAH in the ISM.
Furthermore, the carbon edge is not very sensitive to the size distribution of the grains (Draine, 2003).

4.4.2 Aluminum and calcium

The XIFU simulation shows that dust will be easily detectable, even if the edge itself produced a jump in the spectrum of only few %. However, from the Al edge alone, it would be difficult

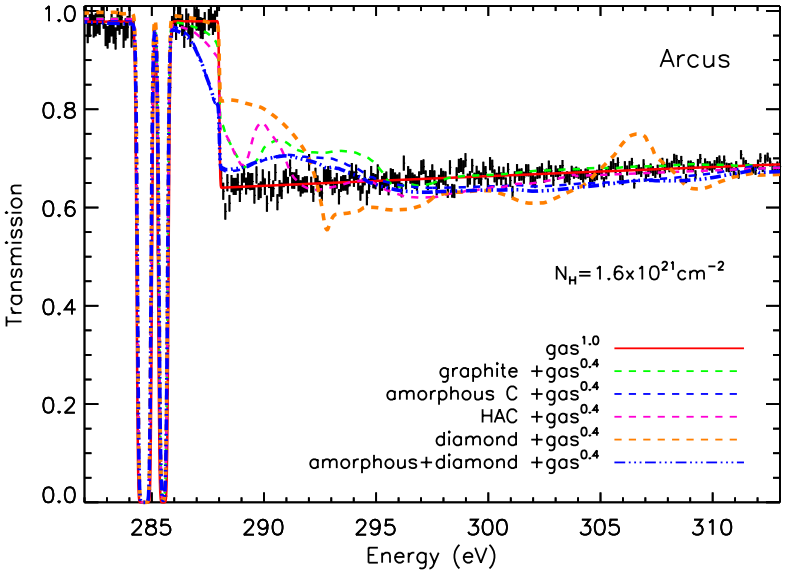

Figure 4.2: A 500 ks simulation of the carbon K-edge, using the Arcus grating, of an XRB in high state ($F_{0.5-2\,\mathrm{keV}} \sim 3 \times 10^{-9}$ erg cm^{-2} s^{-1}). The simulation considers different carbon species, with a dust depletion of 60%. The two absorption lines belong to the atomic phase of C, namely C I.

to distinguish among different compounds.

We also note that contrary to other extinction profiles, the scattering peak, which appears as an emission-like feature before the edge-jump, is noticeable in Al. This peak is sensitive to the dust size distribution (Zeegers et al., 2017) and can be used, in principle, to estimate e.g., the mean grain size along the line of sight. As described above, we also tested the effect of the dust size distribution of Draine and Fraisse (2009) for Al_2O_3. The edge energy of Al lies in a zone sensitive to scattering (Draine, 2003), therefore in Fig. 4.3 the large particles contribution is evident. As shown in Rogantini et al. (2018), the role of a substantial scattering contribution to the extinction not only forces the edge energy to shift, but may also modify the appearance of the edge absorption features. Grains containing seeds of Al and Ca, which are shielded from erosion in the ISM, are believed to be of large size, due to the several layers of coatings surrounding those seeds elements (e.g., Clayton, 1978, and Sect. 4.1.1). With future instruments, we will therefore be able to test also the presence of larger particles for less abundant, but important, constituents of the ISM. The study of the Al edge will be however challenging, as Al is always a major component of X-ray space instruments (often in the form of foils). The extinction feature from Al in the ISM will be always blended with a relatively deep instrumental Al feature. This would need a careful calibration, adding uncertainty to the modeling.

Calcium is totally depleted in the ISM, therefore the main dust features will be detected (Fig. 4.5). However, calcium is mostly contained in silicates and aluminates, where oxygen is the main constituent. XAFS models shows that the first and main absorption feature is due to the nearest neighboring atom that the photoelectron wave will encounter (Lee and

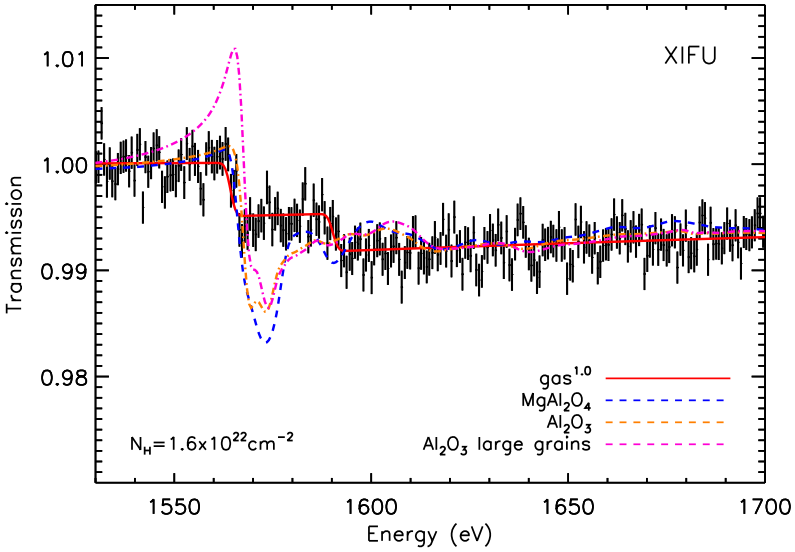

Figure 4.3: A 300 ks simulation of the aluminum K-edge, using the XIFU calorimeter, of the bright XRB GX 3+1 ($F_{2-10\,\mathrm{keV}} \sim 3 \times 10^{-9}$ erg cm^{-2} s^{-1}). The dust depletion is 100%. The data have been binned for clarity.

Ravel, 2005). In the case simulated here, the absorption profile is dominated by oxygen (as is the case, to a lesser extent, in the Al edge), and only at higher energies are the secondary absorption features to be seen. For this reason, the Ca inclusion in a specific silicate may be hard to disentangle through the observed spectrum. However, calcite ($CaCO_3$, dashed orange line), due to its different internal structure, will show a distinctive pattern, which may be in principle disentangled. This will help in determining whether this elusive compound (Kemper et al., 2002) may be present in the ISM. We tested the contribution of possible large grains on anorthite (blue dashed-dotted line in Fig. 4.5). The contribution of larger grains does not produce a well detectable feature.

4.4.3 Sulfur

In the diffuse ISM, sulfur is expected to have a modest depletion (Sect. 4.1.1). We use sulfur in conjunction with iron in the form of troilite, pyrrohtite and pyrite. FeS is a likely candidate for a diffuse interstellar environment, due to its inclusion in GEMS (Bradley, 1994; Bradley et al., 1999). The line of sight towards GX 5-1, at distance of ~9 kpc is likely to cross also molecular clouds and this would apply for any source located near the galactic center. The dust inclusion of sulfur in molecular clouds is still an open issue (Sect. 4.1.1). Some of the S must be associated to ices and carbon-hydrogen aggregates, while the rest may be in the form of FeS or atomic gas. Even the sum of all known S-bearing molecules would be unlikely to exceed few % of the total S abundance. Therefore any significant depletion detected by XARM or XIFU would naturally point to the role of S in GEMS. This amount of S depletion would still not procure visible deviations from the observed total dust spectral energy distribution

(Köhler et al., 2014).

4.4.4 Titanium and nickel

Due to its extremely low abundance in the Universe, titanium will be challenging to detect (Fig. 4.6). Nickel is about twenty times more abundant than Ti, however Ni will be also difficult to study (Fig. 4.7). The large column densities required to produce a Ni edge, will cause also strong absorption by iron, whose K absorption edge lies at 7100 eV, only 1.2 keV away from the one of nickel. Under the conditions of this simulation, the optical depth of iron will be around 18 times larger than the one of nickel. The net effect is that the Ni edge "sees"a continuum which is much lower than the one of the source, reducing the signal to noise ratio in that feature. Both titanium and nickel are however completely depleted in most ISM environments, therefore even a column density estimate will be useful to constrain the abundance of these two elements, which are a product of explosions of both massive stars and white dwarfs.

4.5 Conclusion

In this chapter, we have shown how improved instrumental sensitivity and resolution will help in understanding new aspects of the composition of ID. Our results can be summarized as follows:

Future instruments, with characteristics similar to the Arcus mission, will be able to disentangle between the major components of carbon, namely amorphous carbon (or graphite) and hydrogenated carbon. The effect of minor constituents of C in the ISM (e.g., nano-diamonds and PAH) will be challenging to detect.

Instruments with improved capabilities at energies >2 keV as *Athena*-XIFU or XARM-*Resolve* will be able to determine the main chemical characteristics of elements like Al and Ca. It will be possible in particular to distinguish between calcium in carbonates and silicates, and investigate the dust size distribution of these heavily depleted elements.

Athena-XIFU or XARM-*Resolve* will be able to determine the depletion of sulfur in the ISM. This in turn will help clarify the S inclusion in GEMS, which are sometimes considered as one of the main forms of silicates in the ISM.

Acknowledgements

Dust studies at Leiden Observatory are supported also through the Spinoza Premie of the Dutch science agency, NWO. The Netherlands Institute for Space Research is supported financially by NWO. E.C. and D.R. acknowledge the support of the NWO-VIDI grant 639.042.525. We acknowledge SOLEIL for provision of synchrotron radiation facilities and we would like to thank Delphine Vantelon for assistance in using the LUCIA beamline and Harald Mutschke for procuring the Al-bearing samples. We also thank Alessandra Candian for useful comments on the manuscript. This research made use of the Chandra Transmission Grating Catalog and archive (http://tgcat.mit.edu).

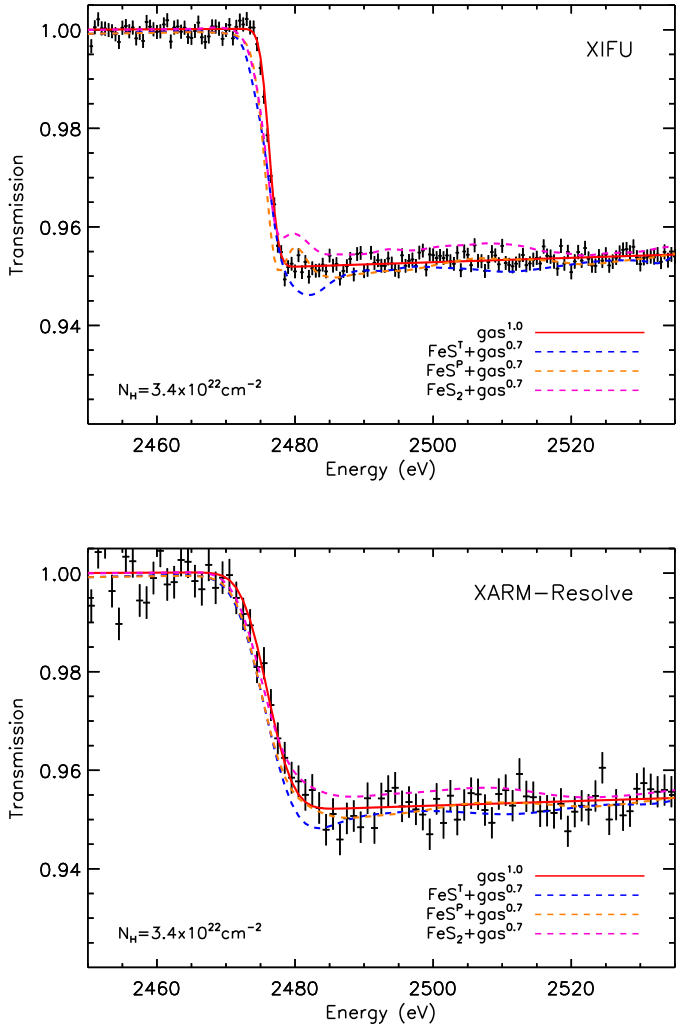

Figure 4.4: Simulation of the sulfur K-edge, using the XIFU calorimeter with an exposure time of 150 ks (top) and XARM-Resolve with a 400 ks exposure time (bottom), of a the bright XRB GX 5–1 ($F_{2-10\,\mathrm{keV}} \sim 2.5 \times 10^{-8}$ erg cm^{-2} s^{-1}). The simulation considers different sulfur species, with a dust depletion of 30%.

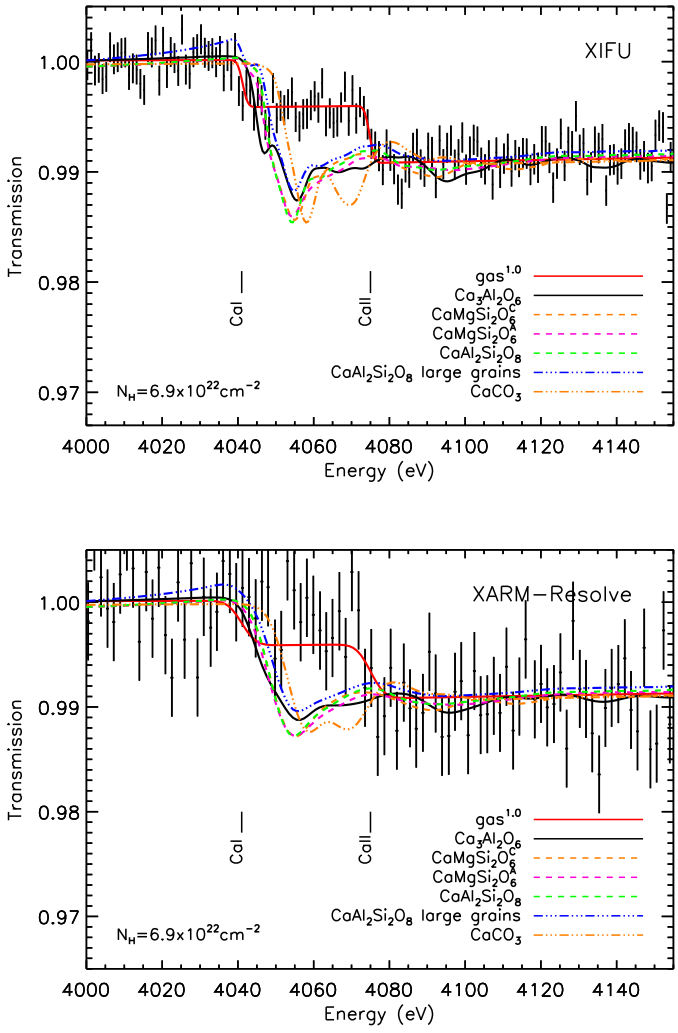

Figure 4.5: Simulation of the calcium K-edge, using the XIFU calorimeter with exposure time 300 ks, (top) and the XARM-Resolve with a 500 ks exposure time (bottom). We used the bright XRB GX 340+00 ($F_{2-10\,\mathrm{keV}} \sim 1.3 \times 10^{-8}$ erg cm^{-2} s^{-1}). The simulation considers different calcium species, with a dust depletion of 100%. The data have been binned for clarity.

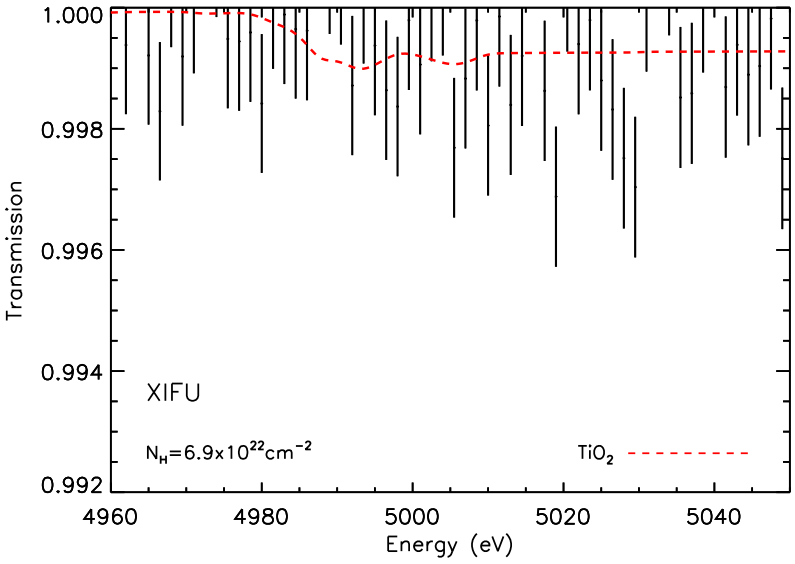

Figure 4.6: A 500 ks simulation of the titanium K-edge, using the XIFU calorimeter, using the bright XRB GX340+00 ($F_{2-10\,\mathrm{keV}} \sim 1.3 \times 10^{-8}\,\mathrm{erg\,cm^{-2}\,s^{-1}}$) as template. The dust depletion is 100%. The data have been binned for clarity.

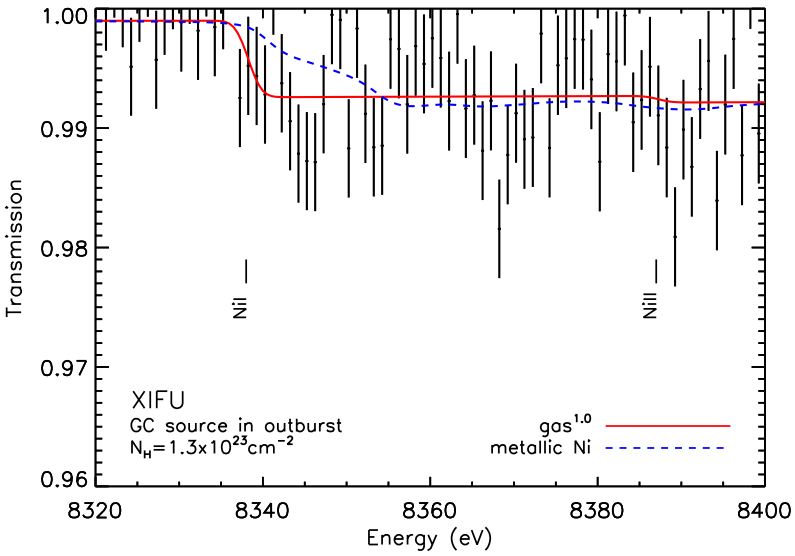

Figure 4.7: A 300 ks simulation of the nickel K-edge, using the XIFU calorimeter, assuming that a highly absorbed source near the GC reaches in outburst the same flux level as GX340+00 ($F_{2-10\,\mathrm{keV}} \sim 1.3 \times 10^{-8}\,\mathrm{erg\,cm^{-2}\,s^{-1}}$). The dust depletion is 100%. The data have been binned for clarity.

4.A Extinction profiles

We show here the extinction profiles in transmission, normalized for the continuum, of the compounds presented in this chapter. Their formula and literature reference is reported in Table 4.1.

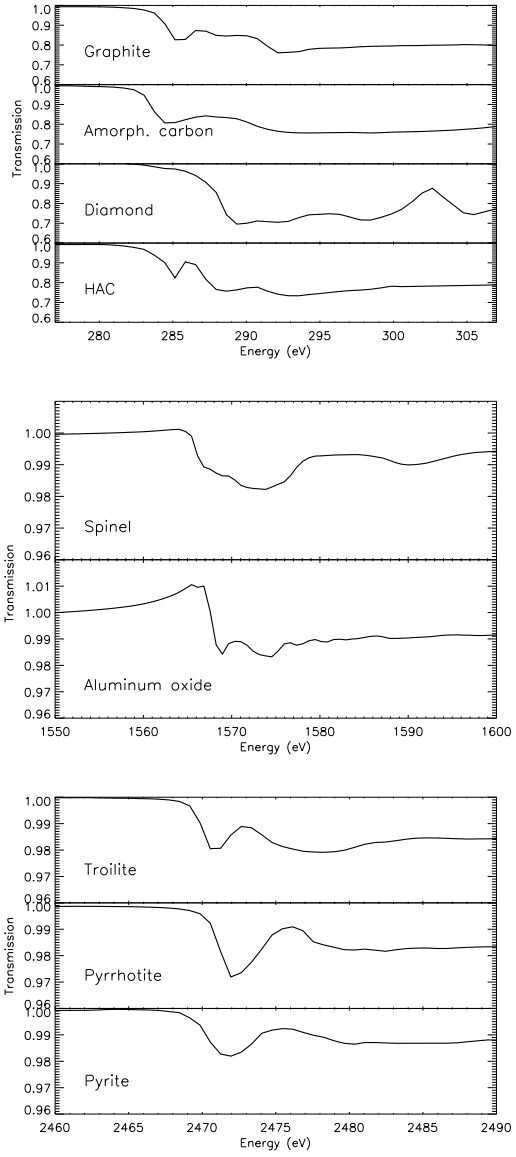

Figure 4.8: The extinction profiles of the C, Al and S compounds presented in this chapter. The dust column densities of the elements are the same used for the simulations. The edge energy is as reported in the literature as well as the original energy resolution.

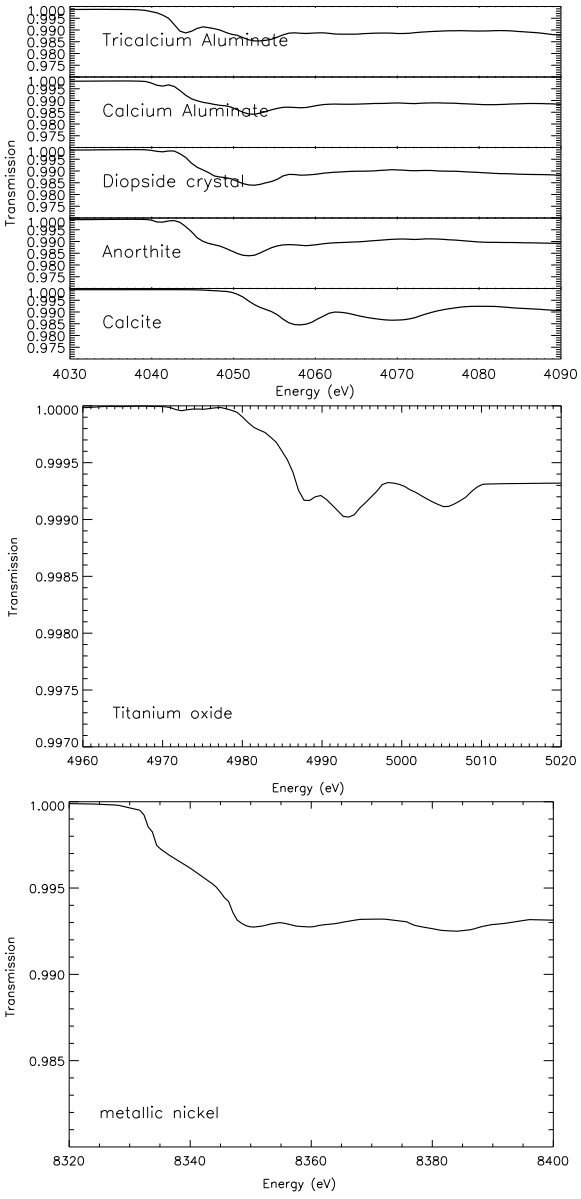

Figure 4.9: The extinction profiles of the Ca, Ti and Ni compounds presented in this chapter. The dust column densities of the elements are the same used for the simulations. The edge energy is as reported in the literature as well as the original energy resolution.

References

Albella, J. M. and Banks, D. K. a. (1998). Composition and Bonding in Amorphous Carbon Films Grown by Ion Beam Assisted Deposition: Influence of the Assistance Voltage. *Diamond and related materials, DRM elsevier*, 215:425–435.

Barret, D., Lam Trong, T., den Herder, J.-W., and et al. (2016). The Athena X-ray Integral Field Unit (X-IFU). In *Space Telescopes and Instrumentation 2016: Ultraviolet to Gamma Ray*, volume 9905, page 99052F.

Bilalbegović, G. and Baranović, G. (2015). Sulphur-bearing species in molecular clouds. *MNRAS*, 446:3118–3129.

Bilalbegović, G., Maksimović, A., and Valencic, L. A. (2018). Tetrahedral hydrocarbon nanoparticles in space: X-ray spectra. *MNRAS*, 476:5358–5364.

Bohren, C. F. (2010). What did kramers and kronig do and how did they do it? *European Journal of Physics*, 31(3):573.

Bonnin-Mosbah, M., Métrich, N., Susini, J., Salomé, M., Massare, D., and Menez, B. (2002). Micro X-ray absorption near edge structure at the sulfur and iron K-edges in natural silicate glasses. *Spectrochimica Acta*, 57:711–725.

Bradley, J. P. (1994). Chemically Anomalous, Preaccretionally Irradiated Grains in Interplanetary Dust From Comets. *Science*, 265:925–929.

Bradley, J. P., Keller, L. P., Snow, T. P., Hanner, M. S., Flynn, G. J., Gezo, J. C., Clemett, S. J., Brownlee, D. E., and Bowey, J. E. (1999). An infrared spectral match between GEMS and interstellar grains. *Science*, 285.

Buijnsters, J. G., Gago, R., Jiménez, I., Camero, M., Agulló-Rueda, F., and Gómez-Aleixandre, C. (2009). Hydrogen quantification in hydrogenated amorphous carbon films by infrared, Raman, and x-ray absorption near edge spectroscopies. *Journal of Applied Physics*, 105(9):093510–093510–7.

Clayton, D. D. (1978). Precondensed matter - Key to the early solar system. *Moon and Planets*, 19:109–137.

Compiègne, M., Verstraete, L., Jones, A., Bernard, J.-P., Boulanger, F., Flagey, N., Le Bourlot, J., Paradis, D., and Ysard, N. (2011). The global dust SED: tracing the nature and evolution of dust with DustEM. *A&A*, 525:A103.

Corrales, L. R., García, J., Wilms, J., and Baganoff, F. (2016). The dust-scattering component of X-ray extinction: effects on continuum fitting and high-resolution absorption edge structure. *MNRAS*, 458:1345–1351.

Costantini, E., Pinto, C., Kaastra, J. S., in't Zand, J. J. M., Freyberg, M. J., Kuiper, L., Méndez, M., de Vries, C. P., and Waters, L. B. F. M. (2012). XMM-Newton observation of 4U 1820-30. Broad band spectrum and the contribution of the cold interstellar medium. *A&A*, 539:A32.

Crinklaw, G., Federman, S. R., and Joseph, C. L. (1994). The depletion of calcium in the interstellar medium. *ApJ*, 424:748–753.

Delgado-Inglada, G., Mesa-Delgado, A., García-Rojas, J., Rodríguez, M., and Esteban, C. (2016). The Fe/Ni ratio in ionized nebulae: clues on dust depletion patterns. *MNRAS*, 456:3855–3865.

Draine, B. (1989). On the Interpretation of the λ 2175 Å Feature. In Allamandola, L. J. and Tielens, A. G. G. M., editors, *Interstellar Dust*, volume 135 of *IAU Symposium*, page 313.

Draine, B. T. (2003). Interstellar Dust Grains. *ARA&A*, 41:241–289.

Draine, B. T. and Fraisse, A. A. (2009). Polarized Far-Infrared and Submillimeter Emission from Interstellar Dust. *ApJ*, 696:1–11.

Duley, W. W., Jones, A. P., and Williams, D. A. (1989). Hydrogenated amorphous carbon-coated silicate particles as a source of interstellar extinction. *MNRAS*, 236:709–725.

Duley, W. W., Millar, T. J., and Williams, D. A. (1980). Interstellar chemistry of sulphur. *MNRAS*, 192:945–957.

Edgar, R. J. and Savage, B. D. (1989). The density distribution of refractory elements away from the Galactic plane. *ApJ*, 340:762–774.

Federman, S. R., Sheffer, Y., Lambert, D. L., and Gilliland, R. L. (1993). Detection of boron, cobalt, and other weak interstellar lines toward Zeta Ophiuchi. *ApJ*, 413:L51–L54.

Ferrarotti, A. S. and Gail, H.-P. (2005). Mineral formation in stellar winds. V. Formation of calcium carbonate. *A&A*, 430:959–965.

Ferrarotti, A. S. and Gail, H.-P. (2006). Composition and quantities of dust produced by AGB-stars and returned to the interstellar medium. *A&A*, 447:553–576.

Field, G. B. (1974). Interstellar abundances: gas and dust. *ApJ*, 187:453–459.

Fitzpatrick, E. L. and Massa, D. (2007). An Analysis of the Shapes of Interstellar Extinction Curves. V. The IR-through-UV Curve Morphology. *ApJ*, 663:320–341.

Gry, C. and Jenkins, E. B. (2017). The nearby interstellar medium toward α Leo. UV observations and modeling of a warm cloud within hot gas. *A&A*, 598:A31.

Henke, B. L., Gullikson, E. M., and Davis, J. C. (1993). X-Ray Interactions: Photoabsorption, Scattering, Transmission, and Reflection at E = 50-30,000 eV, Z = 1-92. *Atomic Data and Nuclear Data Tables*, 54:181–342.

Hoffman, J. and Draine, B. T. (2016). Accurate Modeling of X-ray Extinction by Interstellar Grains. *ApJ*, 817:139.

Hony, S., Waters, L. B. F. M., and Tielens, A. G. G. M. (2002). The carrier of the "30" mu m emission feature in evolved stars. A simple model using magnesium sulfide. *A&A*, 390:533–553.

Hunter, I., Smoker, J. V., Keenan, F. P., Ledoux, C., Jehin, E., Cabanac, R., Melo, C., and Bagnulo, S. (2006). Early-type stars observed in the ESO UVES Paranal Observatory Project - I. Interstellar NaI UV, TiII and CaII K observations*. *MNRAS*, 367:1478–1514.

Jansen, F., Lumb, D., Altieri, B., Clavel, J., Ehle, M., Erd, C., Gabriel, C., Guainazzi, M., Gondoin, P., Much, R., Munoz, R., Santos, M., Schartel, N., Texier, D., and Vacanti, G. (2001). XMM-Newton observatory. I. The spacecraft and operations. *A&A*, 365:L1–L6.

Jenkins, E. B. (2009). A Unified Representation of Gas-Phase Element Depletions in the Interstellar Medium. *ApJ*, 700:1299–1348.

Jenkins, E. B. and Wallerstein, G. (1996). Hubble Space Telescope Observations of Interstellar Lines in Three High-Latitude Stars. *ApJ*, 462:758.

Jiménez-Escobar, A. and Muñoz Caro, G. M. (2011). Sulfur depletion in dense clouds and circumstellar regions. I. H_2S ice abundance and UV-photochemical reactions in the H_2O-matrix. *A&A*, 536:A91.

Jones, A. P., Köhler, M., Ysard, N., Bocchio, M., and Verstraete, L. (2017). The global dust modelling framework THEMIS. *A&A*, 602:A46.

Joseph, C. L., Snow, Jr., T. P., Seab, C. G., and Crutcher, R. M. (1986). Interstellar abundances in dense, moderately reddened lines of sight. I - Observational evidence for density-dependent depletion. *ApJ*, 309:771–782.

Kaastra, J. S., Mewe, R., and Nieuwenhuijzen, H. (1996). SPEX: a new code for spectral analysis of X & UV spectra. In Yamashita, K. and Watanabe, T., editors, *UV and X-ray Spectroscopy of Astrophysical and Laboratory Plasmas*, pages 411–414.

Keller, L. P., Hony, S., Bradley, J. P., Molster, F. J., Waters, L. B. F. M., Bouwman, J., de Koter, A., Brownlee, D. E., Flynn, G. J., Henning, T., and Mutschke, H. (2002). Identification of iron sulphide grains in protoplanetary disks. *Nature* , 417:148–150.

Keller, L. P., Loeffler, M. J., Christoffersen, R., Dukes, C., Rahman, Z., and Baragiola, R. (2010). Irradiation of FeS: Implications for the Lifecycle of Sulfur in the Interstellar Medium and Presolar FeS Grains. In *Lunar and Planetary Science Conference*, volume 41 of *Lunar and Planetary Inst. Technical Report*, page 1172.

Keller, L. P. and Messenger, S. (2008). Relict Amorphous Silicates in Stardust Samples. *Meteoritics and Planetary Science Supplement*, 43:5227.

Kemper, F., Jäger, C., Waters, L. B. F. M., Henning, T., Molster, F. J., Barlow, M. J., Lim, T., and de Koter, A. (2002). Detection of carbonates in dust shells around evolved stars. *Nature* , 415:295–297.

Köhler, M., Jones, A., and Ysard, N. (2014). A hidden reservoir of Fe/FeS in interstellar silicates? *A&A*, 565:L9.

Lee, J. C. and Ravel, B. (2005). Determining the Grain Composition of the Interstellar Medium with High-Resolution X-Ray Spectroscopy. *ApJ*, 622:970–976.

Lee, J. C., Xiang, J., Ravel, B., Kortright, J., and Flanagan, K. (2009). Condensed Matter Astrophysics: A Prescription for Determining the Species-specific Composition and Quantity of Interstellar Dust Using X-rays. *ApJ*, 702:970–979.

Lewis, R. S., Ming, T., Wacker, J. F., Anders, E., and Steel, E. (1987). Interstellar diamonds in meteorites. *Nature* , 326:160–162.

Lodders, K. (2010). Solar System Abundances of the Elements. *Astrophysics and Space Science Proceedings*, 16:379.

Mathis, J. S., Rumpl, W., and Nordsieck, K. H. (1977). The size distribution of interstellar grains. *ApJ*, 217:425–433.

Mie, G. (1908). Beiträge zur Optik trüber Medien, speziell kolloidaler Metallösungen. *Annalen der Physik*, 330:377–445.

Mitsuda, K., Kelley, R. L., Akamatsu, H., Bialas, T., and et al. (2014). Soft x-ray spectrometer (SXS): the high-resolution cryogenic spectrometer onboard ASTRO-H. In *Space Telescopes and Instrumentation 2014: Ultraviolet to Gamma Ray*, volume 9144 of *Proc. SPIE*, page 91442A.

Nandra, K., Barret, D., Barcons, X., Fabian, A., den Herder, J.-W., Piro, L., Watson, M., Adami, C., Aird, J., Afonso, J. M., and et al. (2013). The Hot and Energetic Universe: A White Paper presenting the science theme motivating the Athena+ mission. *ArXiv e-prints*.

Neuville, D. R., Cormier, L., Roux, J., de Ligny, D., Flank, A.-M., Henderson, G. S., and Lagarde, P. (2007). An In Situ High Temperature Investigation of Cation Environments in Aluminate and Silicate Glasses and Liquids at the LUCIA Beamline. In Hedman, B. and Pianetta, P., editors, *X-ray Absorption Fine Structure - XAFS13*, volume 882 of *American Institute of Physics Conference Series*, pages 413–415.

Pinto, C., Kaastra, J. S., Costantini, E., and de Vries, C. (2013). Interstellar medium composition through X-ray spectroscopy of low-mass X-ray binaries. *A&A*, 551:A25.

Pinto, C., Kaastra, J. S., Costantini, E., and Verbunt, F. (2010). High-resolution X-ray spectroscopy of the interstellar medium. XMM-Newton observation of the LMXB GS 1826-238. *A&A*, 521:A79.

Rehr, J. J. and Albers, R. C. (2000). Theoretical approaches to x-ray absorption fine structure. *Reviews of Modern Physics*, 72:621–654.

Reitsma, G., Boschman, L., Deuzeman, M. J., González-Magaña, O., Hoekstra, S., Cazaux, S., Hoekstra, R., and Schlathölter, T. (2014). Deexcitation Dynamics of Superhydrogenated Polycyclic Aromatic Hydrocarbon Cations after Soft-x-Ray Absorption. *Physical Review Letters*, 113(5):053002.

Reitsma, G., Boschman, L., Deuzeman, M. J., Hoekstra, S., Hoekstra, R., and Schlathölter, T. (2015). Near edge X-ray absorption mass spectrometry on coronene. *J. Chem. Phys.*, 142(2):024308.

Rogantini, D., Costantini, E., Zeegers, S. T., de Vries, C. P., Bras, W., de Groot, F., Mutschke, H., and Waters, L. B. F. M. (2018). Investigating the interstellar dust through the Fe K-edge. *A&A*, 609:A22.

Schneider, P. C. and Schmitt, J. H. M. M. (2010). X-raying the AU Microscopii debris disk. *A&A*, 516:A8.

Sembach, K. R. and Savage, B. D. (1996). The Gas and Dust Abundances of Diffuse Halo Clouds in the Milky Way. *ApJ*, 457:211.

Shin, S. I., Go, A., Kim, I. Y., and et al. (2013). A beneficial role of exfoliated layered metal oxide nanosheets in optimizing the electrocatalytic activity and pore structure of pt-reduced graphene oxide nanocomposites. *Energy Environ. Sci.*, 6:608.

Siebenmorgen, R. and Krügel, E. (2010). The destruction and survival of polycyclic aromatic hydrocarbons in the disks of T Tauri stars. *A&A*, 511:A6.

Smith, R. K., Abraham, M. H., Allured, R., Bautz, M., Bookbinder, J., and et al. (2016). Arcus: the x-ray grating spectrometer explorer. In *Space Telescopes and Instrumentation 2016: Ultraviolet to Gamma Ray*, volume 9905 of *Proc. SPIE*, page 99054M.

Snow, T. P., Destree, J. D., and Jensen, A. G. (2007). The Abundance of Interstellar Fluorine and Its Implications. *ApJ*, 655:285–298.

Snow, Jr., T. P. (1975). The depletion of interstellar elements and the interaction between gas and dust in space. *ApJ*, 202:L87–L90.

Sofia, U. J. and Jenkins, E. B. (1998). Interstellar Medium Absorption Profile Spectrograph Observations of Interstellar Neutral Argon and the Implications for Partially Ionized Gas. *ApJ*, 499:951–965.

Stern, E. A., Newville, M., Ravel, B., Yacoby, Y., and Haskel, D. (1995). The UWXAFS analysis package: philosophy and details. *Physica B Condensed Matter*, 208:117–120.

Tielens, A. G. G. M. (2001). The Composition of Circumstellar and Interstellar Dust. In Woodward, C. E., Bicay, M. D., and Shull, J. M., editors, *Tetons 4: Galactic Structure, Stars and the Interstellar Medium*, volume 231 of *Astronomical Society of the Pacific Conference Series*, page 92.

Tielens, A. G. G. M. (2013). The molecular universe. *Reviews of Modern Physics*, 85:1021–1081.

Tielens, A. G. G. M., Seab, C. G., Hollenbach, D. J., and McKee, C. F. (1987). Shock processing of interstellar dust - Diamonds in the sky. *ApJ*, 319:L109–L113.

Trivedi, B. M. P. and Larimer, J. W. (1981). A semiempirical model for heavy element depletion in the interstellar medium. *ApJ*, 248:563–568.

Turner, B. E. (1991). Observations and chemistry of interstellar refractory elements. *ApJ*, 376:573–598.

Valencic, L. A. and Smith, R. K. (2013). Interstellar Abundances toward X Per, Revisited. *ApJ*, 770:22.

Van Kerckhoven, C., Tielens, A. G. G. M., and Waelkens, C. (2002). Nanodiamonds around HD 97048 and Elias 1. *A&A*, 384:568–584.

Van Loon, L. L., Throssell, C., and Dutton, M. D. (2015). Comparison of nickel speciation in workplace aerosol samples using sequential extraction analysis and x-ray absorption near-edge structure spectroscopy. *Environ. Sci.: Processes Impacts*, 17:922–931.

Verner, D. A., Ferland, G. J., Korista, K. T., and Yakovlev, D. G. (1996). Atomic Data for Astrophysics. II. New Analytic FITS for Photoionization Cross Sections of Atoms and Ions. *ApJ*, 465:487.

Vidal, T. H. G., Loison, J.-C., Jaziri, A. Y., Ruaud, M., Gratier, P., and Wakelam, V. (2017). On the reservoir of sulphur in dark clouds: chemistry and elemental abundance reconciled. *MNRAS*, 469:435–447.

Voit, G. M. (1992). Destruction and survival of polycyclic aromatic hydrocarbons in active galaxies. *MNRAS*, 258:841–848.

Wakelam, V. and Herbst, E. (2008). Polycyclic Aromatic Hydrocarbons in Dense Cloud Chemistry. *ApJ*, 680:371–383.

Wasson, J. T. (1985). *Meteorites: Their record of early solar-system history*.

Weisskopf, M. C. (1999). The Chandra X-Ray Observatory (CXO): An Overview. *ArXiv Astrophysics e-prints*.

Welty, D. E. and Crowther, P. A. (2010). Interstellar TiII in the Milky Way and Magellanic Clouds. *MNRAS*, 404:1321–1348.

Westphal, A. J., Stroud, R. M., Bechtel, H. A., and et al. (2014). Evidence for interstellar origin of seven dust particles collected by the Stardust spacecraft. *Science*, 345:786–791.

Whittet, D. C. B., editor (2003). *Dust in the galactic environment*.

Whittet, D. C. B. (2011). Spectropolarimetry of Interstellar Dust and Ice Features. In Bastien, P., Manset, N., Clemens, D. P., and St-Louis, N., editors, *Astronomical Polarimetry 2008: Science from Small to Large Telescopes*, volume 449 of *Astronomical Society of the Pacific Conference Series*, page 93.

Wiscombe, W. J. (1980). Improved mie scattering algorithms. *Appl. Opt.*, 19(9):1505–1509.

Wooden, D. H. (2008). Cometary Refractory Grains: Interstellar and Nebular Sources. *Space Sci. Rev.*, 138:75–108.

Zeegers, S. T., Costantini, E., de Vries, C. P., Tielens, A. G. G. M., Chihara, H., de Groot, F., Mutschke, H., Waters, L. B. F. M., and Zeidler, S. (2017). Absorption and scattering by interstellar dust in the silicon K-edge of GX 5-1. *A&A*, 599:A117.